1 Supplementary material

1.1 Table of notations in the derivation

We present a table of descriptions of all notations we used in Table S1.

Table S1: This table contains descriptions of notations in the derivation.

Notations	Descriptions of notations
N	Number of locations in a target area
l	Each location in a target area
k	Number of normalizing flows ($k = 1 \cdots K$)
z_i	Unobserved variable
z_{0i}	Leak node
r_i^0	Auxiliary variable for each target unobserved variable z_i.
μ_i, σ_i	Parameters for the normal distribution for the auxiliary variable r_i^0
$\phi(\cdot), \delta(\cdot)$	Mapping functions that generate μ_i, σ_i
q_i	The approximate posterior distributions of the unobserved variable z_i
α_i	Prior distribution for the unobserved variable z_d
$\mathcal{P}(i)$	Parents node of node z_i
ϵ_i	Environmental noises on node z_i
w_{ij}	Weight that quantify the quantitative relations from node z_i to z_j
w_{ϵ_i}	Weight that quantify the quantitative relations from ϵ_i to z_i
w_{0i}	Weight that quantify the quantitative relations from leak node z_{0i} to z_i
g	Binary XOR node that demonstrates the exclusive relation between two nodes
x	Observed variable
ϵ_x	Environmental noises on node z_x
w_{jx}	Weight that quantify the quantitative relations from parent node $j \in \mathcal{P}(x)$ to x
w_{ϵ_x}	Weight that quantify the quantitative relations from ϵ_x to x
$f(\cdot)$	Normalizing flow transformation function
M	Sample size to generate q_i from $r_i^K \sim q(r_i^K)$ by Monte Carlo method
$\tau = \{\mathbf{v}_i, \mathbf{u}_i, b_i\}$	Free parameters in the planar flow transformation for variable i
w_g	Weight that quantify the quantitative relations from the XOR node g to child nodes of g
$\mathcal{L}_v$	Variational lower bound
$\mathcal{L}_t$	Triplet Loss
β	Margin parameter to constrain the differences of dissimilarity in the triplet loss
$\mathcal{L}$	Final objective function
ρ, λ	Hyperparameters for weight update

1.2 Table S2: Evaluation results using synthesized data from real InSAR imagery

The AUC of the test posterior models with different flow numbers K and the prior model is shown in Table S2.

Table S2: This table contains the evaluation results using synthesized data from real InSAR imagery. We present the AUC of the test posterior models with different NGA means no ground truth label is available.

Event	**Model**	AUC_{LS}	AUC_{BD}	AUC_{LF}
Haiti	$k = 0$	0.9584	0.9690	NGA
	$k = 1$	0.9633	0.9713	NGA
	$k = 3$	0.9696	0.9756	NGA
	$k = 5$	0.9781	0.9821	NGA
	$k = 7$	0.9872	0.9857	NGA
	$k = 8$	**0.9904**	**0.9920**	NGA
	$k = 9$	0.9882	0.9845	NGA
	Prior	0.9408	0.8300	NGA
Puerto Rico	0	0.9314	0.9720	0.9690
	$k = 1$	0.9504	0.9815	0.9124
	$k = 2$	0.9618	0.9868	0.9586
	$k = 3$	0.9870	0.9894	0.9665
	$k = 4$	**0.9903**	**0.9939**	**0.9899**
	$k = 5$	0.9899	0.9904	0.9894
	Prior	0.9158	0.7050	0.8662
Hokkaido	0	0.9446	NGA	NGA
	$k = 1$	0.9693	NGA	NGA
	$k = 2$	0.9807	NGA	NGA
	$k = 3$	**0.9894**	NGA	NGA
	$k = 4$	0.9855	NGA	NGA
	Prior	0.9166	NGA	NGA

1.3 Figure S1: Example of synthesized DPM with different flow number

Figure S1 shows the visualization of DPMs in the 2021 Haiti earthquake on the focused area in Figure 2(a). We present the real-world DPM Figure S1(a) generated by the ARIA team [1], the synthesized DPMs (b), (c), (d) generated from our test posterior models with flow number K = 0, 3, 8 and (e) generated from our DisasterVINF model.

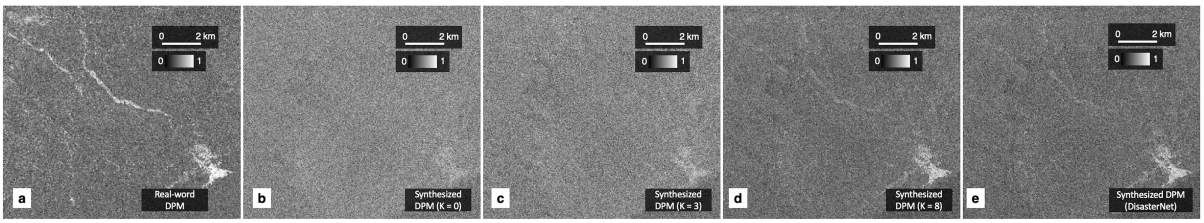

Figure S1: Visualization of DPMs in the focused area in Figure 2 in the 2021 Haiti earthquake. (a) shows the real-world DPM generated by the ARIA team [1]. (b)-(d) show the synthesized DPMs generated from our test posterior models with flow number K = 0, 3, 8. (d) shows the synthesized DPM generated from our DisasterVINF model.

1.4 Figure S2: Example of distribution changes using normalizing flows

We present an example of changes in normalizing flow distributions for landslides in the 2021 Haiti earthquake case Figure S2.

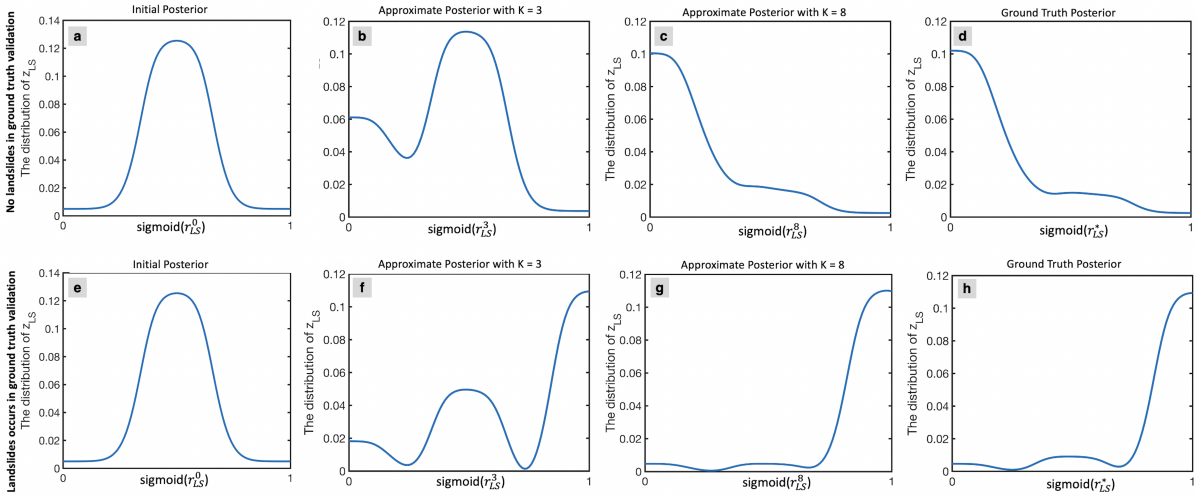

Figure S2: An example of changes in normalizing flow for landslide distributions modeling in the 2021 Haiti earthquake case. (a)-(c) and (e) - (g) present the distribution transformations. A logit-normal distribution (a), (e) is transformed to a highly complex distribution (c), (g), which approximates better the true posteriors in (d), (h), respectively. (a)-(d) is obtained for a location that was later verified no landslides occurred while (e)-(h) are for a location with landslides occurrence.

1.5 Figure S3: Characterization of our framework performance on synthesized data

We present the characterization of our framework performance on synthesized data. The evaluation of the negative variational lower bound on synthesized data is shown in Figure S3 (a). Figures S3(b)(c)show ROC curves for the prior model, DisasterVINF model, and test posterior models with different flow numbers for landslide and building damage models in the 2021 Haiti earthquake, respectively.

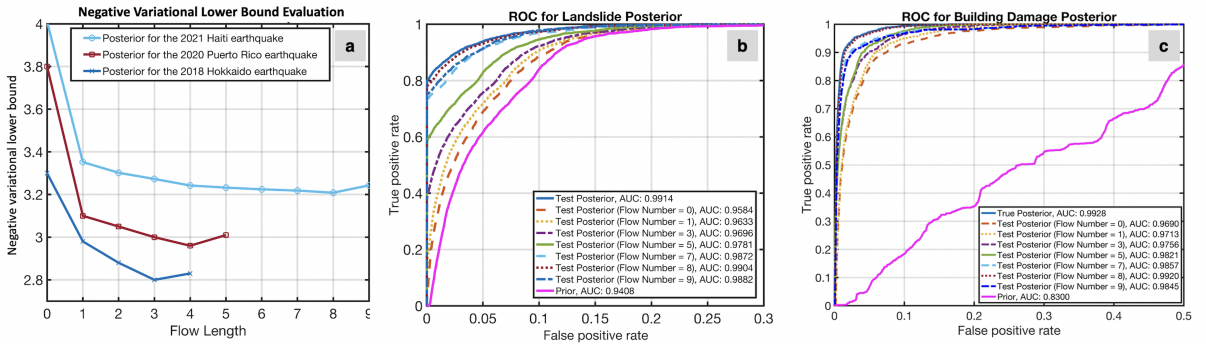

Figure S3: Characterization of our framework performance on synthesized data. (a) shows the evaluation of the negative variational lower bound on synthesized data. (b)(c)show ROC curves for the prior model, DisasterVINF model, and test posterior models with different flow numbers for landslide and building damage models in the 2021 Haiti earthquake, respectively.

1.6 Figure S4: ROC curves for different models in the 2020 Puerto Rico earthquake event

We present the ROC curves for different LS, LF, and BD models in the 2020 Puerto Rico earthquake event are shown in Figure S4.

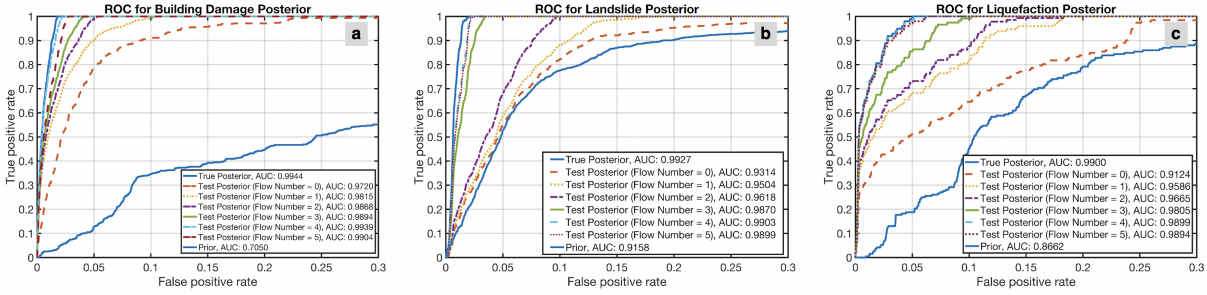

Figure S4: Figure (a) shows the ROC curves of the prior building damage model, our DisasterVINF model, and test posterior models with different flow numbers. Figures (b) and (c) show the ROC curves of the prior landslide and liquefaction model from the USGS, our DisasterVINF model, and test posterior models with different flow numbers, respectively.

1.7 Table S3: Ablation study examining the effectiveness of sample size M

Table S3 below presents the sensitivity study for sample size M, showing how changes in sample size during the Monte Carlo sampling steps (as per Algorithm 1, line 10) affect the model's accuracy, as indicated by AUC values.

Table S3: Sample size evaluation using synthesized data from real InSAR imagery. M represents the model sample size. NGA means no ground truth label is available.

	Haiti EQ.			Puerto Rico EQ.			Hokkaido EQ.		
M	AUC_{LS}	AUC_{LF}	AUC_{BD}	AUC_{LS}	AUC_{LF}	AUC_{BD}	AUC_{LS}	AUC_{LF}	AUC_{BD}
$M = 10$	0.7912	0.8057	NGA	0.8042	0.7993	0.7744	0.8069	NGA	NGA
$M = 100$	0.8632	0.8612	NGA	0.8513	0.8665	0.9569	0.8693	NGA	NGA
$M = 1,000$	0.9799	0.9861	NGA	0.9789	0.9791	0.9667	0.9778	NGA	NGA
M **= 5,000**	**0.9904**	**0.9920**	**NGA**	**0.9903**	**0.9939**	**0.9899**	**0.9894**	**NGA**	**NGA**
$M = 10,000$	0.9906	0.9919	NGA	0.9907	0.9941	0.9895	0.9896	NGA	NGA

1.8 Table S4: Ablation study evaluating the effectiveness of update size ρ

The results of our ablation study for weight update size are illustrated in Table S4.

Table S4: Weight update size evaluation using synthesized data from real InSAR imagery. ρ is the weight update size. NGA means no ground truth label is available.

	Haiti EQ.			Puerto Rico EQ.			Hokkaido EQ.		
ρ	AUC_{LS}	AUC_{LF}	AUC_{BD}	AUC_{LS}	AUC_{LF}	AUC_{BD}	AUC_{LS}	AUC_{LF}	AUC_{BD}
$\rho = 0.0001$	0.9741	0.9729	NGA	0.9815	0.9771	0.9424	0.9777	NGA	NGA
$\rho = 0.001$	0.9809	0.9818	NGA	**0.9903**	**0.9939**	**0.9899**	0.9819	NGA	NGA
$\rho = 0.01$	**0.9904**	**0.9920**	NGA	0.9843	0.9881	0.9796	**0.9894**	NGA	NGA
$\rho = 0.1$	0.9762	0.9734	NGA	0.9764	0.9802	0.9695	0.9773	NGA	NGA
$\rho = 1$	0.9698	0.9592	NGA	0.9324	0.9219	0.9199	0.9323	NGA	NGA
$\rho = 5$	0.8913	0.8881	NGA	0.8218	0.8190	0.8201	0.8915	NGA	NGA
$\rho = 10$	0.7812	0.7994	NGA	0.7539	0.7496	0.7401	0.7401	NGA	NGA

1.9 Table S5: Evaluation of effectiveness of components in our DisasterVINF framework

Table S5 shows AUC and negative variational lower bound (NVLB) values, with higher AUC and lower NVLB indicating better performance.

Table S5: Evaluation of effectiveness of components in our DisasterVINF framework using synthesized data from real InSAR imagery. We present AUC values and negative variational lower bound (NVLB) of the 2020 Puerto Rico earthquake events.

Method	AUC_{LS}	AUC_{LF}	AUC_{BD}	NVLB
VI Full	0.9906	0.9901	0.9897	2.9559
VI Local	**0.9903**	**0.9939**	**0.9899**	**2.9561**
MCMC Full	0.9812	0.9705	0.9743	3.1023
MCMC Local	0.9621	0.9499	0.9515	3.4125